

Submitted to ApJ

# Spectral Slope Variability of BL Lac Objects in the Optical Band

Fausto Vagnetti

*Dipartimento di Fisica, Università di Roma “Tor Vergata”,  
Via della Ricerca Scientifica 1, I-00133 Roma (Italy)*

Dario Trevese, and Roberto Nesci

*Dipartimento di Fisica, Università di Roma “La Sapienza”,  
Piazzale A. Moro 2, I-00185 Roma (Italy)*

## ABSTRACT

Light curves of eight BL Lac objects in the BVRI bands have been analyzed. All of the objects tend to be bluer when brighter. However spectral slope changes differ quantitatively from those of a sample of QSOs analyzed in a previous paper (Trevese & Vagnetti 2002) and appear consistent with a different nature of the optical continuum. A simple model representing the variability of a synchrotron component can explain the spectral changes. Constraints on a possible thermal accretion disk component contributing to the optical luminosity are discussed.

*Subject headings:* galaxies: active - BL Lacertae objects: general - BL Lacertae objects: individual (3C 66A, PKS 0422+004, S5 0716+71, OJ 287, ON 231, OQ 530, S5 1803+78, BL Lac) - quasars: general

## 1. INTRODUCTION

Multi-wavelength observations of active galactic nuclei (AGN) suggest the presence of various emission components with different relative weights in different AGN classes. The large number of parameters involved in physical models of emission mechanisms can hardly be constrained by single epoch observations. Multi-band variability studies are then crucial in identifying and constraining individual components. Moreover, active nuclei are not spatially resolved in general. For this reason variability time scales, delays and correlations between variations in different continuum components or emission lines provide the main information about the location of different components. The very definition of AGN classes is in part

based on variability properties. In fact, while quasars (QSOs) and Seyfert galaxies vary, on average, less than 0.5 mag on time scales of months in the optical band, blazars (i.e. BL Lac objects and Optically Violent Variables, OVVs) may change their luminosities by more than one mag in a few days (Ulrich, Maraschi, and Urry 1997). Quantifying spectral variability will then help understanding different AGN classes by comparison. Although monitoring campaigns, from radio to X-ray wavelengths, exist for a limited number of objects, they are difficult to realize with adequate time sampling and duration. For this reason we try to exploit multi-band variability studies limited to the optical range, which in some case are available for several objects and relatively long observing periods. In a previous paper Trevese & Vagnetti (2002) analyzed the spectral slope variability of a sample of PG QSOs on the basis of the light curves in the B and R bands, provided by the Wise Observatory group, who monitored 42 quasars for 7 years with a typical sampling interval of about one month (Giveon et al. 1999). A spectral variability parameter  $\beta \equiv \Delta\alpha/\Delta \log f_\nu$ ,  $f_\nu$  being the specific flux and  $\alpha \equiv \partial \log f_\nu / \partial \log \nu$  the spectral slope, was defined by Trevese & Vagnetti (2002) who derived constraints on variability mechanisms from the average  $\alpha$  and  $\beta$  values. In particular they showed that the variation of spectral slope implied by changes of the accretion rate are not able to explain  $\beta$  values deduced from the observations, while “hot spots” on the accretion disc, possibly caused by instability phenomena (Kawaguchi et al. 1998), can easily account for the observed spectral variability. In the present study we analyze B, V, R, I light curves of eight BL Lac objects obtained by D’Amicis et al. (2002) in a monitoring campaign of about 5 years with an average sampling interval of  $\approx 25$  days. We show that BL Lacs clearly differ from QSOs in their  $\alpha, \beta$  distribution. We show that a simple model representing the variability of a synchrotron component can account for the observed  $\alpha$  and  $\beta$  values and we discuss constraints which can be derived from spectral variability on the amount of thermal radiation contributed by a disk component in the optical band.

## 2. DATA ANALYSIS

The sample consists of 8 radio selected BL Lac objects listed in Table 1. Observations were made in the period 1995-1999, in the standard Johnson-Cousins B, V, R, I bands and are described in D’Amicis et al. (2002). Typical photometric uncertainties range from 0.01 to 0.03 mag r.m.s.. In table 1 the following quantities are reported: *Column 1* Name; *Column 2* Coordinate Designation; *Column 3* Number of observations; *Column 4* average B magnitude; *Column 5* redshift; *Column 6* average spectral slope; *Column 7* spectral variability index. For the present analysis we regard as “simultaneous” the observations in different bands taken during the same observing night. We considered the data dereddened as in D’Amicis et al. (2002). We then define for each object an “instantaneous” slope by a straight line fit through

the B, V, R, I data points as a function of  $\log \nu$ , neglecting for the moment any curvature of the spectral energy distribution within the optical range. A positive correlation of the instantaneous spectral slope  $\alpha \equiv \partial \log f_\nu / \partial \log \nu$  with flux changes  $\delta \log f_{\nu_R}$  has been already discussed by D’Amicis et al. (2002). In the present paper we quantify spectral variations in two different ways. A first method considers, for each object, all the positions in the  $\alpha - \log f_{\nu_B}$  diagram,  $f_{\nu_B}$  being the specific flux at the effective frequency  $\nu_B$  of the blue band. These points, together with the relevant regression lines are shown in Figure 1 for each of the 8 objects. In the same figure the solid lines represent the average increase of  $\alpha$  with  $\log f_{\nu_B}$ . Clearly this quantity is independent of the time of occurrence of different  $\alpha$  and  $\log f_{\nu_B}$  values. We now refer to the blue band, instead than the red one used by D’Amicis et al. (2002) in their correlation analysis, for comparison with the study of QSO spectral variations by Trevese & Vagnetti (2002). The slopes  $b$  of the regression lines of each object, can be assumed as a first spectral variability index.

A second method, adopted by Trevese & Vagnetti (2002) considers, for each object, the quantity:

$$\beta_{ij} \equiv \beta(\tau_{ij}) \equiv \frac{\alpha_j - \alpha_i}{\log f_{\nu_B}(t_j) - \log f_{\nu_B}(t_i)}, \quad \tau_{ij} \equiv \frac{(t_j - t_i)}{(1 + z)}, i, j = 1, N \quad (1)$$

which represents the change of spectral slope per unit variation of  $\log$  flux as a function of the rest frame time lag  $\tau_{ij}$  and again we refer to the flux changes in the blue band. We stress that  $\beta$  is a very sensitive indicator of spectral changes but, for this reason, it is also a noisy quantity. For flux changes comparable or smaller than the photometric noise,  $\beta$  values are randomly spread over a wide range. Thus we limit the computation to  $|\log f_{\nu_B}(t_j) - \log f_{\nu_B}(t_i)| > 0.03$ . In any case, instead of individual  $\beta_{ij}$  values, it’s worth referring to average values, e.g. in bins of time lag  $\tau$ .

To constrain physical models of variability, it’s interesting to see whether spectral changes are different on different time scales. Figure 2 shows for each object  $\beta_{ij}$  as a function of  $\tau_{ij}$ . The average values of  $\beta_{ij}$  in bins of 200 days are also shown. For each object the value of the first spectral variability index  $b$  is also shown for comparison. In general the larger variations of  $\beta$  occur at larger time lags where, due to the worst statistic, they are less reliable. For  $\tau \lesssim 500$  d there are no evident systematic trends of  $\beta$  as a function of  $\tau$ . Thus it makes sense to define a less noisy index taking the average of  $\beta$  within the first 500 days:

$$\beta \equiv \langle \beta_{ij} \rangle, \quad \tau_{ij} < 500 \text{ d}. \quad (2)$$

In the following we limit our analysis to the average variability index  $\beta$ .

Besides the spectral slope  $\alpha$  computed by a straight line fit through the  $\log f_{\nu_i}$  versus  $\log \nu_i$  (i=B,V,R,I) data points, we also computed two other slope values, towards the blue

and red side of the spectral range:

$$\alpha_{BR} = \frac{0.4[(B - R) - (B_o - R_o)]}{\log(\lambda_B/\lambda_R)} - 2, \quad \alpha_{VI} = \frac{0.4[(V - I) - (V_o - R_o)]}{\log(\lambda_V/\lambda_I)} - 2,$$

where  $B_o, V_o, R_o, I_o$  and  $\lambda_B, \lambda_V, \lambda_R, \lambda_I$  are the zero points and the effective wavelengths of the four photometric bands (Cox 2000). For all but two objects the values of  $\alpha_{VI}$  and  $\alpha_{BR}$  are respectively slightly larger and slightly smaller, on average, than  $\alpha$ , indicating a little curvature of the spectrum, and the slopes of the linear regressions  $\alpha_{BR}$  vs.  $\alpha$  and  $\alpha_{VI}$  vs.  $\alpha$  do not differ significantly from one. In the case of BL Lac and OQ 530,  $\alpha_{VI}$  is almost equal to  $\alpha_{BR}$ , or slightly smaller, and becomes significantly smaller than  $\alpha$  (and  $\alpha_{BR}$ ) when  $\alpha$  is small. A possible explanation is that the (constant) contribution of the host galaxy emerges in the faint phases causing a more marked softening of the spectrum on the red side of the wavelength interval considered. This is consistent with the fact that the host galaxy contribution, as reported by Urry et al. (2000), is relatively strong for these two objects.

## 2.1. Comparison with QSOs

The average values  $\beta$  of the variability index, for all time lags smaller than 500 days rest-frame, are plotted in Figure 3 versus the relevant average  $\alpha$  values. For comparison the values for the sample of 42 quasars discussed by Trevese & Vagnetti (2002) are also shown<sup>1</sup>. BL Lacs and quasars are clearly segregated in the  $\alpha - \beta$  plane. BL Lacs show, on average, lower  $\alpha$  values, consistently with the absence, or lower relative weight, of the thermal blue bump component. The new information in Figure 3 is that BL Lacs have  $\beta$  values smaller, on average, than quasars. BL Lac variability is stronger,  $\alpha$  changes are also larger, but their ratio  $\beta$  is smaller. Moreover, using both  $\alpha$  and  $\beta$  parameters together allows a clear distinction of the two classes. We want to discuss whether this behavior fits into the currently accepted models describing the different emission mechanisms of blazars and QSOs.

# 3. VARIABILITY OF THE SYNCHROTRON COMPONENT

## 3.1. A simple model

The continuum spectral energy distribution of blazars from radio frequencies to X and  $\gamma$ -rays can be explained by a synchrotron emission plus inverse Compton scattering (Ghis-

---

<sup>1</sup> $\beta$  values for QSOs are slightly different from those shown in Trevese & Vagnetti (2002) since they have been recomputed at a fixed *rest-frame* time lag interval.

ellini & Maraschi 1992; Sikora, Begelman, & Rees 1994). Variability can be produced by an intermittent channeling into the jet of the energy produced by the central engine. Spada et al. (2001) have considered a detailed model where crossing of different shells of material, ejected with different velocities, produce shocks which heat the electrons responsible for the synchrotron emission. The resulting spectra are compared with multi-band, multi-epoch observations of 3C 279 from radio to  $\gamma$  frequencies, showing a good agreement. Similar computations have been done for Mkn 421 (Guetta et al. 2002). In the case of the eight objects of our sample, B, V, R, I bands are sampling variability of the synchrotron component. This component can be roughly described by a broken power law characterized by the break (or peak in  $\nu L_\nu$ ) frequency  $\nu_p$  and the asymptotic spectral slopes  $\alpha_1$  and  $\alpha_2$  at low and high frequency respectively,  $\alpha_1 > -1$ ,  $\alpha_2 < -1$  (Tavecchio, Maraschi, & Ghisellini 1998). An equivalent representation is:

$$L_\nu = L_p \cdot 2\left[\left(\frac{\nu}{\nu_p}\right)^{-\alpha_1} + \left(\frac{\nu}{\nu_p}\right)^{-\alpha_2}\right]^{-1} \equiv L_p \cdot H(\nu/\nu_p; \alpha_1, \alpha_2) \quad (3)$$

where  $L_p$  is the specific luminosity at  $\nu_p$ . We adopt this representation for a stationary component of the SED and we add to it a second (variable) component with the same analytical form but different peak frequency  $\nu_{p'}$  and amplitude  $L_{p'}$  to produce spectral changes:

$$L_\nu = L_p \cdot H(\nu/\nu_p; \alpha_1, \alpha_2) + L_{p'} \cdot H(\nu/\nu_{p'}; \alpha_1, \alpha_2) \quad (4)$$

The addition of the second component mimics the behavior of the synchrotron emission of model spectra when shell crossing occurs, producing an increment of emission with  $\nu_{p'} > \nu_p$ , due to newly accelerated electrons. With such a representation we can compute  $\alpha$  and  $\beta$  as a function of  $\nu_{p'}/\nu_p$ , for different values of  $\nu_p$  and given values of  $\alpha_1$ ,  $\alpha_2$  and  $L_{p'}/L_p$ . We adopt typical values of the asymptotic slopes  $\alpha_1 = -0.5$ ,  $\alpha_2 = -2$ , we assigned to  $\nu_p$  different values in the range  $2.5\text{--}10 \cdot 10^{14}$  Hz, we made  $\nu_{p'}/\nu_p$  vary in the range 0.8–4 and we adopted a ratio  $L_{p'}/L_p$  corresponding to a 0.5 mag change in the blue band, which is representative of the r.m.s. variability. The results are shown in Figure 4, where we use as  $\alpha$  the slope of the stationary component. The three different lines are computed for  $\log \nu_p = 14.4, 14.7, 15.0$  from left to right respectively. The computed curves fall naturally in the region occupied by the data, namely it is possible to account for the position of the objects in the  $\alpha - \beta$  plane with typical values of  $\alpha_1$ ,  $\alpha_2$ ,  $\nu_{p'}/\nu_p$  and  $\nu_p$ , required to represent the overall SED of the objects considered (see fos98).

### 3.2. The Thermal Bump

BL Lac objects can be classified according to the break frequency of synchrotron emission, from Low frequency peaked BL Lacs (LBL) which show a break in the IR/optical band to High frequency peaked BL Lacs (HBL) with the synchrotron break at UV/X-ray (or higher) energies (Padovani et al. 1995). On average the blue bump (TB) produced by the accretion disk tends to be negligible in HBLs while in LBLs its contribution may be important. According to Cavaliere & D’Elia (2001) this can be interpreted in terms of higher accretion rate  $\dot{m}$  in the case of LBLs, producing a stronger thermal emission from the disk, while HBLs are dominated by non-thermal energy, partly extracted from rotational energy of the central Kerr hole.

In particular the TB remains negligible during changes of the synchrotron component in the case of Mkn 421, a classic HBL, while emerges clearly during the faint phases in the case of 3C 279, a classic LBL (see Spaans & Guillian 2002). We stress that the TB is relatively “narrow”, since its emission is mostly concentrated in the UV region, while the synchrotron emission extends from radio frequencies to the UV (or X-rays). Then the change of relative intensity of the two components can produce strong changes of the spectral slope in the optical-UV region, where the synchrotron and TB components have very different slopes ( $\approx -2$  and  $\approx +1.5$  respectively). As a result, in the case of LBL we should find strongly negative  $\beta$  values in the faint phases, namely a hardening instead of a softening of the spectrum, at wavelengths smaller but close to the peak of the TB, as observed in the case of 3C 279, where we can estimate  $\beta \simeq -1$  at  $\lambda \simeq 2500 \text{ \AA}$  on the basis of the data reported by Pian et al. (1999) (see their Figure 4). However these negative  $\beta$  values do not seem to be typical in the case of our sample, although synchrotron breaks are distributed in the frequency range  $10^{13} - 10^{15} \text{ Hz}$ . Thus, in principle, we can set upper limits to contribution of the accretion disk to the overall SED on the basis of the observed  $\beta$  values. For a rough estimate it is sufficient to approximate the TB with a black body emission. As already noted in §1, although the TB itself may vary, possibly due to instabilities which produce hot spots in the accretion disk (Trevese & Vagnetti 2002), the amplitudes of its variations are smaller than those of blazars (see Trevese et al. 1994). Thus we can approximately consider TB emission as a constant during the much larger variations of the synchrotron component.

Thus we consider a specific luminosity  $L_s \equiv L(\nu, t)$  of the synchrotron component with a time dependent local slope  $\alpha_s(t)$  at the observing frequency  $\nu = \bar{\nu}$ , and a constant thermal TB luminosity  $L_{TB}$  with local slope  $\alpha_{TB}$ . The total specific luminosity at two times  $t$  and  $t_o$  will be  $L = L_s + L_{TB}$  and  $L_o = L_{so} + L_{TB}$  respectively. The local spectral slope  $\alpha$  of the

composite SED is:

$$\alpha \equiv \frac{\partial \log L}{\partial \log \nu} = \frac{L_s}{L} \alpha_s + \frac{L_{TB}}{L} \alpha_{TB} \quad (5)$$

Defining  $\chi = \frac{L_{TB}}{L_{so}}$ ,  $\varepsilon = \frac{L_s}{L_{so}}$  and  $\delta = \alpha_s - \alpha_{so}$ , where the subscript “o” indicates the initial time, we have  $\beta_s = \delta / \log \varepsilon$  for the “unperturbed” synchrotron component and:

$$\beta \equiv (\alpha - \alpha_o) / \log \frac{L}{L_o} = \left[ \frac{\varepsilon}{\varepsilon + \chi} \delta + \frac{\chi(\varepsilon - 1)}{(\varepsilon + \chi)(1 + \chi)} (\alpha_o - \alpha_{TB}) \right] / \log \frac{\varepsilon + \chi}{1 + \chi} \quad (6)$$

for the composite spectrum. In Figure 5 we report the spectral variability index  $\beta$  as a function of  $\chi$  for different values of the temperature  $T$ .

We assume a typical value  $\alpha_{so} = -1.75$  and we assume for the disk a black body temperature  $T = 10^4 K$  or  $T = 2 \times 10^4 K$ . In both cases we compute  $\beta$  as a function of  $\chi$ , for two values of  $\eta$  and a typical value  $\beta_s = 1$ . The result is shown in Figure 5. For 3C 279 we can estimate (Pia99)  $\beta \approx -1$ ,  $\chi \approx 1$  and  $T \approx 2 \times 10^4 K$  which is consistent with the relevant curve in the figure. It appears that e.g. the condition  $\beta > 0.5$  implies  $\chi \lesssim 0.4$  for  $T = 10^4 K$ , or  $\chi \lesssim 0.2$  for  $T = 2 \times 10^4 K$ . Similarly  $\beta > 0$  implies  $\chi \lesssim 1$  for  $T = 10^4 K$ , or  $\chi < 0.5$  for  $T = 2 \times 10^4 K$ .

#### 4. SUMMARY AND CONCLUSIONS

We have performed a new analysis of the light curves of eight BL Lac objects monitored in B,V,R,I bands for a total period of about 5 years with an average sampling interval of  $\approx 25$  days.

Adopting a spectral variability index  $\beta$ , representing the average ratio between the change of spectral slope and the logarithmic luminosity change, we find that BL Lacs show smaller spectral variability respect to quasars (analyzed in a previous paper). This happens despite both the spectral slope and luminosity variations of BL Lacs are larger then those of QSOs. BL Lacs and QSOs appear clearly segregated in the  $\alpha - \beta$  plane. Our analysis allows a quantitative comparison of the observations with a model based on variability of the synchrotron component. The model easily accounts for the observed position in the  $\alpha - \beta$  plane with a natural choice of the relevant parameters. Thus the segregation in the  $\alpha - \beta$  plane is a consequence of the different emission mechanism in the optical band: synchrotron in the case of BL Lacs and thermal hot spots on the accretion disk in the case of QSOs (see Tre02). A strong thermal bump can produce negative  $\beta$  values, which are not observed in our sample, while do in fact appear in some typical LBL object, where the thermal bump emerges in the faint phases. Thus spectral variability, even restricted to the optical band,

can be used to set limits on the relative contribution of the synchrotron component and the thermal component to the overall SED. Further studies of the spectral variability index  $\beta$  in different objects will allow to establish whether the thermal bump is significant only in the most extreme LBL, or to what extent its contribution, possibly correlated with the accretion rate  $\dot{m}$ , is related to total luminosity.

We wish to thank Alfonso Cavaliere and Enrico Massaro for discussion and comments, and Silvia Sclavi for providing details on photometric calibrations. This work was partly supported by MIUR under grant COFIN 2001/028773.

## REFERENCES

- D’Amicis, R., Nesci, R., Massaro, E., Maesano, M., Montagni, F., D’Alessio, F., 2002, PASA, 19, 111
- Cavaliere, A., & D’Elia, V., 2002, ApJ, 571, 226
- Cox, A. N. , 2000, Allen’s Astrophysical Quantities (Berlin: Springer)
- Fossati, G, Maraschi, L., Celotti, A., Comastri, A., & Ghisellini, G., 1998, MNRAS, 299,433
- Maraschi, L., Ghisellini, G., & Celotti, A., 1992, ApJ, 377,403
- Giveon, U., Maoz, D., Kaspi, S., Netzer, H., & Smith P. S. 1999, MNRAS, 306, 637
- Guetta, D., Ghisellini, G., Lazzati, D., & Celotti, A., 2002, proc. 5th AGN Italian Workshop, 2001, Mem. SAIIt (in press) (astro-ph/0210115)
- Kawaguchi, T., Mineshige, S., Umemura, M., & Turner, E. L. 1998, ApJ, 504, 671
- Padovani, P., & Giommi, P., 1995, ApJ, 444, 567
- Pian, E. et al., 1999, ApJ, 521, 112
- Sikora, M., Begelman, M. & Rees, M.J., 1994, ApJ, 421, 153
- Spada, M., Ghisellini, G., Lazzati, D., & Celotti, A., 2001, MNRAS, 325, 1559
- Tavecchio, F., Maraschi, L., & Ghisellini, G., 1998, ApJ, 509, 608
- Trevese, D., Kron, R.G., Majewski, S.R., Bershad, M.A., Koo, D.C., 1994, ApJ, 433, 494



Trevese, D., & Vagnetti, F., 2002, ApJ, 564, 624

Ulrich MH, Maraschi L., & Urry C. M. 1997, ARA&A, 35, 445

Urry, M., Scarpa, R., O’Dowd, M., Falomo, R., Pesce, J. H., & Treves, A., 2000, ApJ, 532, 816

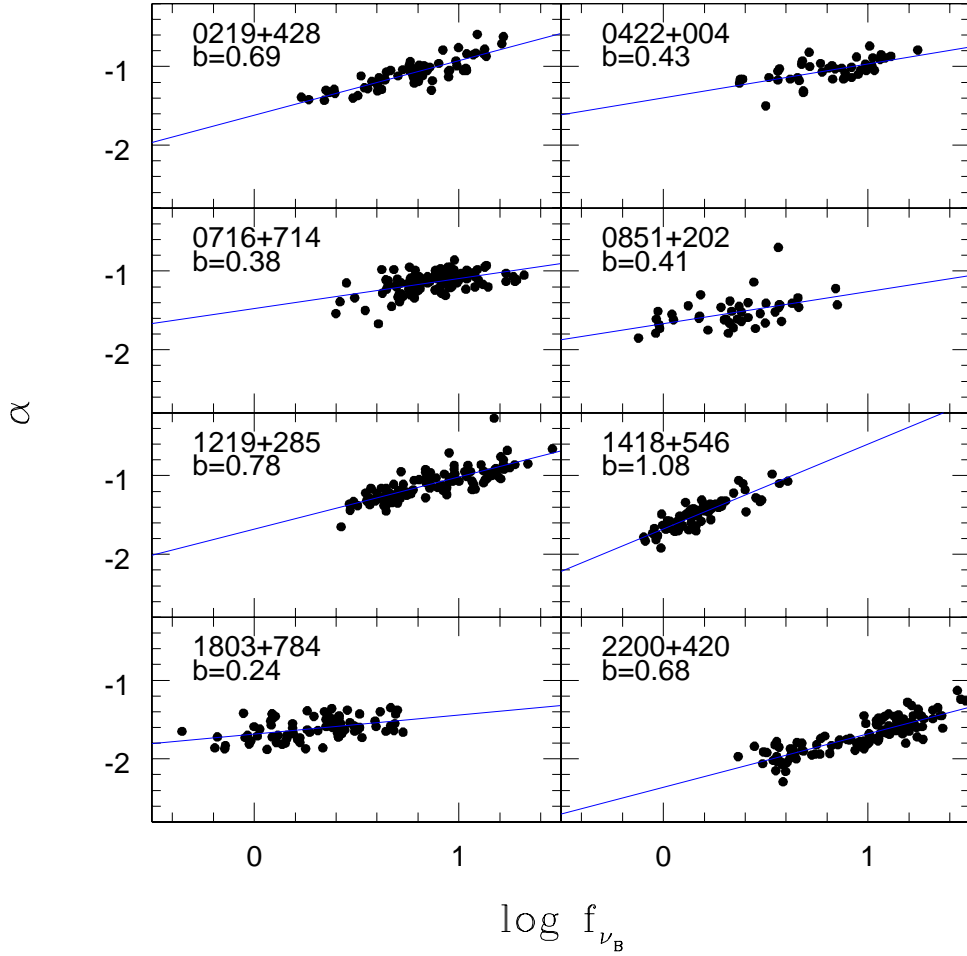


Fig. 1.— Instantaneous spectral slope  $\alpha$  versus specific flux at the effective frequency of the observed blue band, for the eight objects of the sample. The regression lines are also shown. The slopes  $b$ , reported in the relevant panels, can be adopted as a first spectral variability indicator.

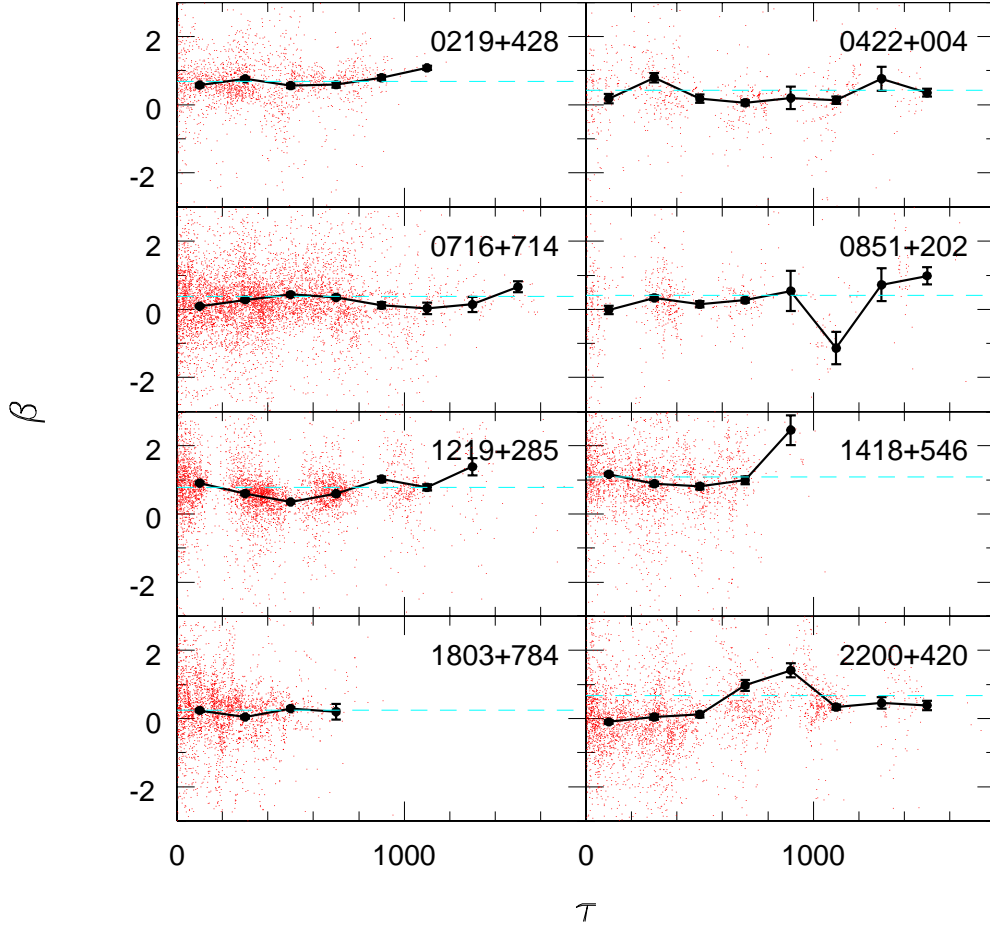


Fig. 2.—  $\beta_{ij}$  as a function of  $\tau_{ij}$  for each object in the sample. Large dots represent the mean values of  $\beta_{ij}$  in bins of 200 days. Error bars represent the standard deviation of the mean. The dashed lines correspond the first spectral variability indicator  $b$ .

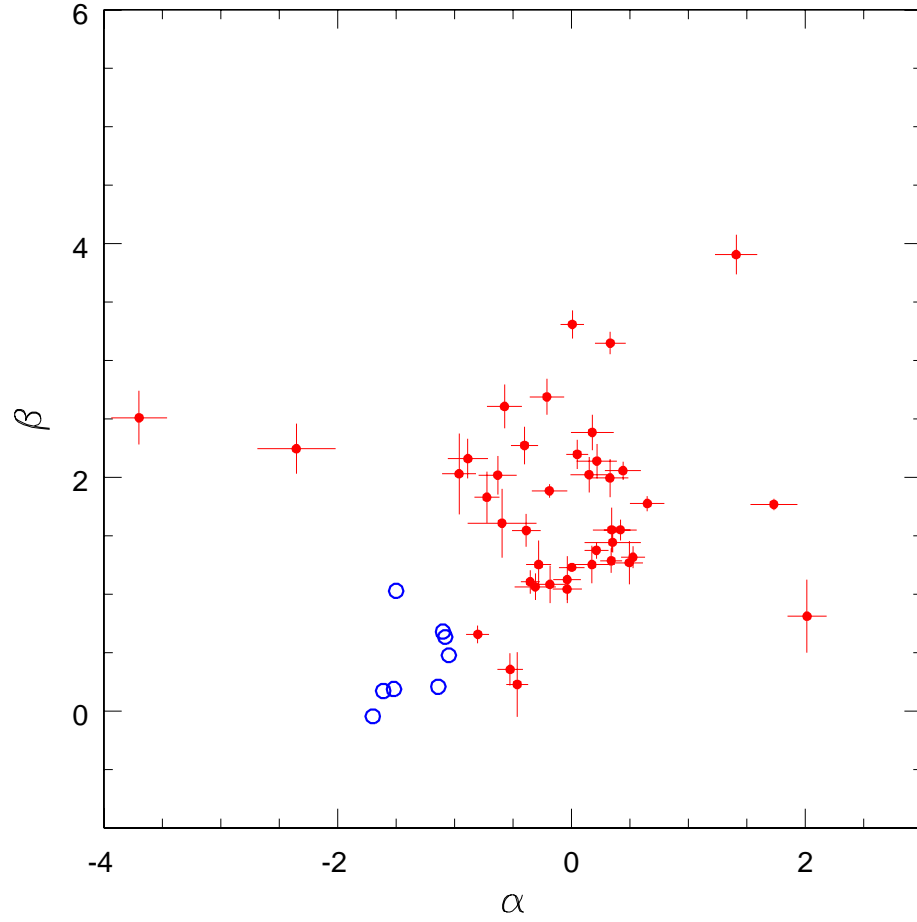


Fig. 3.— The average values  $\beta$  of the variability index versus the average spectral slope for the eight objects of the BL Lacs sample (*open circles*) and the 42 QSOs (*?, see*]tre02 (*dots*).

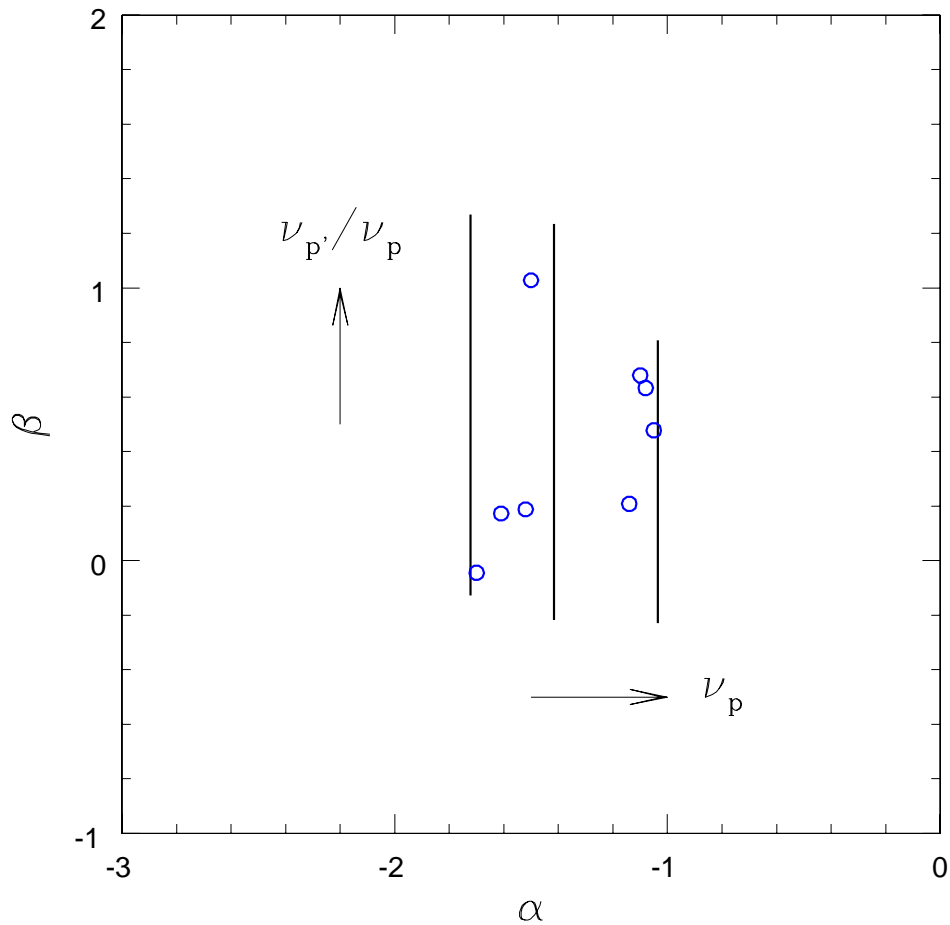


Fig. 4.— Spectral variability index  $\beta$  versus spectral slope. Open circles represent BL Lac objects as in Figure 3. Lines represent the models. Each line corresponds to a fixed value of  $\nu_P$ :  $\log \nu_P = 14.4, 14.7, 15.0$ . Along each line the ratio  $\nu_{P'}/\nu_P$  varies from 0.8 to 4 (from bottom to top). We adopted an  $L_{P'}/L_P$  ratio corresponding a magnitude change of 0.5 mag.

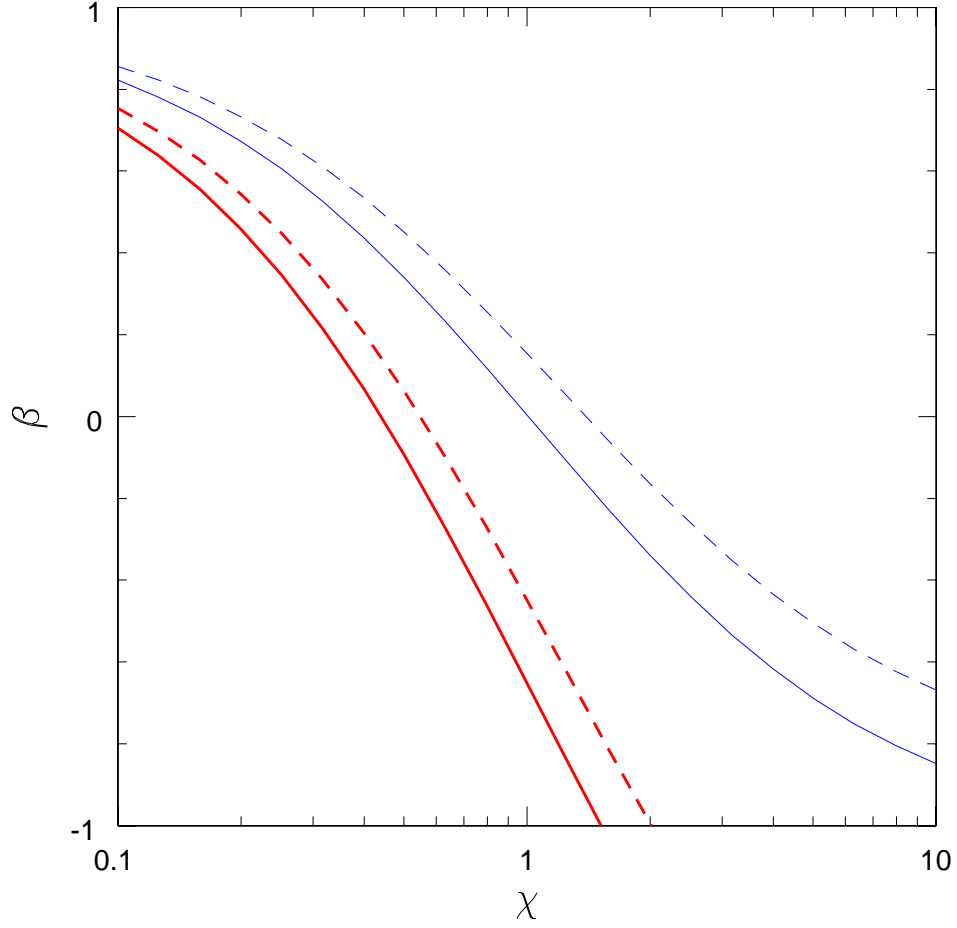


Fig. 5.— Spectral variability versus the ratio between the thermal bump and synchrotron components at the observing frequency:  $\chi = \frac{L_{TB}}{L_{so}}$ . The curves have been computed for two values of the thermal component temperature  $T = 2 \cdot 10^4$  K (*thick lines*) and  $T = 10^4$  K (*thin lines*), and for  $\varepsilon = 1.1$  (*continuous lines*)  $\varepsilon = 1.5$  (*dashed lines*).

Table 1. The sample of BL Lac objects.

Name	Coord. Desig.	$N_{obs}$	B	$z$	$\alpha$	$\beta$
3C 66A	0219+428	66	15.01	0.444	-1.08	0.63
PKS 0422+004	0422+004	44	15.00	-	-1.05	0.48
S5 0716+71	0716+714	118	14.51	-	-1.14	0.21
OJ 287	0851+202	44	15.83	0.306	-1.52	0.19
ON 231	1219+285	101	14.50	0.102	-1.10	0.68
OQ 530	1418+546	74	16.22	0.152	-1.50	1.03
S5 1803+78	1803+784	84	16.07	0.680	-1.61	0.17
BL Lac	2200+420	120	15.56	0.069	-1.70	-0.04